Mineral-induced bubbling effect and biomineralization as strategies to create highly porous and bioactive scaffolds for dentin tissue engineering

Camila Correa da Silva Braga de Melo[1], Fernanda Balestrero Cassiano[1], Érika Soares Bronze-Uhle[1], Vitor de Toledo Stuani[1], Ester Alves Ferreira Bordini[1], Marjorie de Oliveira Gallinari[2], Carlos Alberto de Souza Costa[2], Diana Gabriela Soares[1]

[1]Department of Operative Dentistry, Endodontics and Dental Materials, Sao Paulo University – USP, Bauru School of Dentistry, Bauru, SP, Brazil

[2]Department of Physiology and Pathology, Univ. Estadual Paulista – UNESP, Araraquara School of Dentistry, Araraquara, SP, Brazil

Corresponding author:
Prof. Dr. Diana Gabriela Soares
Department of Operative Dentistry, Endodontics and Dental Materials,
Bauru School of Dentistry, University of Sao Paulo (USP), Sao Paulo, Brazil
Alameda Octavio Pinheiro Brisolla, 9-75
17012-901 Bauru, SP, BRAZIL
E-mail: dianasoares@fob.usp.br

ACKNOWLEDGMENTS

This work was supported by the Fundação de Amparo à Pesquisa do Estado de São Paulo (FAPESP) – Grant/Award Numbers 2016/15674-5 and 2019/06884-4, and by the Coordenação de Aperfeiçoamento de Pessoal de Nível Superior - Brasil (CAPES) - Finance Code 001.

ABSTRACT

The objective of the study was to assess the biological and mechanical characteristics of chitosan-based scaffolds enriched by mineral phases and biomineralized in Simulated Body Fluid (SBF) as a possible biomaterial for dentin regeneration. Thus, porous chitosan scaffolds were prepared by the mineral-induced bubbling-effect technique and subjected to biomineralization to create biomimetic scaffolds for dentin tissue engineering. Suspensions containing calcium hydroxide, nanohydroxyapatite, or β-tricalcium phosphate were added to the chitosan (CH) solution and subjected to gradual freezing and freeze-drying to obtain CH-Ca, CH-nHA, and CH-βTCP porous scaffolds, respectively, by the bubbling effect. Then, scaffolds were incubated in SBF for 5 days at 37°C, under constant stirring, to promote calcium-phosphate (Ca-P) biomineralization. Scanning electron microscopy revealed increased pore size and porosity degree on mineral-containing scaffolds, with CH-Ca and CH-nHA presenting as round, well-distributed, and with an interconnected pore network. Nevertheless, incubation in SBF disrupted the porous architecture, except for CH-Ca_{SBF}, leading to the deposition of Ca-P coverage, confirmed by Fourier Transform Infrared Spectroscopy analyses. All mineral-containing and SBF-treated formulations presented controlled degradation profiles and released calcium throughout 28 days. When human dental pulp cells (HDPCs) were seeded onto scaffold structures, the porous and interconnected architecture of CH-Ca, CH-nHA, and CH-Ca_{SBF} allowed cells to infiltrate and spread throughout the scaffold structure, whereas in other formulations cells were dispersed or agglomerated. It was possible to determine a positive effect on cell proliferation and odontogenic differentiation for mineral-containing formulations, intensely improved by biomineralization. A significant increase in mineralized matrix deposition (by 8.4 to 18.9 times) was observed for CH-Ca_{SBF}, CH-nHA_{SBF}, and CH-βTCP_{SBF} in comparison with plain CH. The bioactive effect on odontoblastic marker expression (ALP activity and mineralized matrix) was also observed for HDPCs continuously cultivated with conditioned medium obtained from scaffolds. Therefore, biomineralization of chitosan scaffolds containing different mineral phases was responsible for increasing the capacity for mineralized matrix deposition by pulpal cells, with potential for use in dentin tissue engineering.

KEYWORDS

Scaffold, chitosan, mineral, biomineralization, dentin, vital pulp therapy

1 | INTRODUCTION

Direct pulp-capping is a vital pulp therapy (VPT) that involves the application of biomaterials over the exposed pulp in an attempt to achieve tissue regeneration mediated by the intrinsic regenerative potential of resident dental pulp stem cells. This therapy aims to recover and maintain normal function and vitality of this tissue through the odontoblastic differentiation and deposition of dentin by these cells, creating a mineralized barrier capable of sealing pulp from exposure (da Rosa et al., 2018; Zaen El-Din et al., 2020). Calcium hydroxide and calcium silicate cements/powder have been widely used for applications in VPT. However, their solubility, lack of adhesion, and low mechanical properties are considered concerns for long-term maintenance. Also, direct contact with these materials results in superficial necrosis and inflammation in remnant pulp tissue, resulting in a disorganized reparative process and establishment of a mineralized barrier with defects that may compromise dental pulp vitality. Therefore, tissue-engineering strategies have been proposed in the field of regenerative dentistry to overcome these clinical issues relative to current VPT techniques (da Rosa et al., 2018; Widbiller & Schmalz, 2021).

Dentin tissue-engineering proposes the development of materials with the ability to induce dentin repair/regeneration through the activation of the tertiary dentinogenesis process from resident pulpal and periapical stem cells, in a cell-homing pathway (Widbiller & Schmalz, 2021; Soares, Bordini, Swanson, de Souza Costa, & Bottino, 2021). Scaffolds play a crucial role in this process, since they serve as a framework for tissue neo-genesis. Moreover, they must modulate the chemotaxis events of resident cells to their structure, followed by their adhesion, spreading, infiltration, proliferation, cell differentiation, and the stimulation of secretory activity (Piva, Silva, & Nör, 2014; Galler, Eidt, & Schmalz, 2014; Soares et al., 2018a). In this sense, biomaterials with a composition similar to that of dentin have been proposed as an alternative to direct pulp-capping. Chitosan-based scaffolds demonstrate cytocompatibility and bioactivity with dental pulp cells, allowing for adequate cell interaction and inducing the processes of chemotaxis and mineralized matrix deposition in vitro and in vivo (Li, Liu, Zhao, Wu, & Xu, 2014; Soares et al., 2018a). The chemical composition of chitosan has shown an affinity for anionic biomolecules, such as the glycosaminoglycans of host extracellular matrix, and also allows for various possibilities for covalent and ionic modifications, including the incorporation of calcium and phosphate to create biomimetic scaffolds for mineralized tissue regeneration, thus adding the characteristic of versatility to this

biopolymer (Madihally & Matthew, 1999; Ribeiro, Vieira, Melo, Araújo, & Lima, 2017; Islam, Shahruzzaman, Biswas, Nurus Sakib, & Rashid, 2020).

In addition to chemical composition, the three-dimensional (3D) architecture of scaffolds is critical to the regenerative process. Thus, scaffolds with a high degree of porosity and structure with interconnected pores are essential for favoring regeneration (Wei & Ma, 2006; Soares et al., 2018b; Soares, Bordini, Swanson, de Souza Costa, & Bottino, 2021). Chitosan solutions can be easily processed into porous scaffolds by phase-separation. Although widely used, this technique does not provide adequate control of pore size and interconnectivity (Madihally & Matthew, 1999; Pestov & Bratskaya, 2016). However, a bubbling-effect technique developed by our group facilitated the creation of an ordered and interconnected macro-pore network in chitosan scaffolds (Soares et al., 2020). Calcium hydroxide was incorporated into chitosan solution, acting as a CO_2 source upon carbonation and reaction with acetic acid, increasing pore diameter and total porosity during the gradual freezing procedure (Soares et al., 2020). The macro-porous structure obtained after freeze-drying allowed cells from surrounding in vitro 3D-matrices and in vivo tissues to easily infiltrate and spread inside and throughout the scaffold structure, denoting its potential as an inductive cell-homing platform (Soares et al., 2021). Furthermore, calcium was complexed to chitosan, creating the chitosan-calcium (CH-Ca) scaffold, which also acted as a calcium-release system capable of increasing the odontogenic potential of human dental pulp cells by increasing the deposition of mineralized tissue (Soares et al., 2020).

Based on the results obtained by our group, we hypothesized that other mineral phases could also promote the bubbling effect, generating a conductive surface that would favor tissue formation and growth. In this context, calcium phosphates have been extensively studied as biomaterials for their favorable characteristics such as biocompatibility, bioactivity, the absence of toxicity, variable degradation rates, and osteoconductivity (Guastaldi & Aparecida, 2010). For this reason, scaffolds containing hydroxyapatite (HA) [$Ca_{10}(PO_4)_6(OH)_2$] and β-tricalcium phosphate (βTCP) [$Ca_3(PO_4)_2$] have been investigated in tissue engineering, and their applications have also been suggested for targeting odontogenic differentiation (AbdulQader, Kannan, Rahman, Ismail, & Mahmood, 2015; Li et al., 2020; Cao et al., 2020; Guerrero-Gironés et al., 2021). This addition can improve the uniformity of osteoblastic cell-spreading and bone tissue formation when compared with that in non-combined materials, because the similarity to a bone/dentin extracellular matrix leads to enhanced interaction with precursor cells, as well as increasing the expression of some important bone markers, such as osteocalcin and bone sialoprotein, and improving the mechanical strength of

scaffolds (Zhang & Ma, 2004; Kasten et al., 2008; Liu, Holzwarth, & Ma, 2012; Kim et al., 2015; AbdulQader, Kannan, Rahman, Ismail, & Mahmood, 2015; Goodarzi, Hashemi-Najafabadi, Baheiraei, & Bagheri, 2019; Wang, Lin, & Kang, 2019; Guerrero-Gironés et al., 2021).

Surface morphology should also be taken into consideration because it will exert a direct impact on cell adhesion, proliferation, and differentiation. An increase in the capacity for mineralized tissue deposition has already been demonstrated when mesenchymal stem cells adhere to surfaces with defined topography compared with smooth surfaces (Hu et al., 2010; Zhang, Hu, & Ma, 2012). The incubation of scaffolds in Simulated Body Fluid (SBF), a solution with composition, pH, temperature, and ionic concentration similar to those of human blood plasma, has been used as a biomineralization technique to modify the surfaces of scaffolds through the deposition of partially carbonated hydroxyapatite, mimicking the biological process of bone and tooth formation (Kokubo & Takadama, 2006). This biomimetic approach aims to modify the internal pore walls without changing the structure and properties of the scaffolds (Zhang & Ma, 2004; Wei & Ma, 2006). In this sense, this process can be used as a simple surface-modification technique for scaffolds used in bone and dentin tissue-engineering (Murphy, Kohn, & Mooney, 2000; Zhang & Ma, 2004).

Since the inorganic portion of dentin consists of mineral salts in the form of hydroxyapatite crystals, and calcium-based materials have been used for mineralized tissue regeneration, it can be suggested that the addition of mineral phases such as calcium hydroxide, HA, and βTCP to chitosan scaffolds, followed by biomineralization in SBF, could increase the bioactive potential of these biomaterials. Therefore, the objective of this work was to develop chitosan-based scaffolds enriched by mineral phases and biomineralized in SBF capable of activating the dentinogenic phenotype on human dental pulp cells, leading to dentin repair.

2 | MATERIALS AND METHODS

2.1 | Formulation and characterization of scaffolds

2.1.1 | *Synthesis of scaffolds*

All solutions described in this section are from the same manufacturer (Sigma-Aldrich Corporation, St. Louis, MO, USA), and the fabrication process followed the bubbling-effect technique established by our group (Soares et al., 2020). A solution of 2% (w/v) high-molecular-weight CH (310,000-375,000 Da; 75-80% deacetylated; pH 3.5) was

prepared by the dissolution of chitosan powder in 2% (v/v) acetic acid solution under stirring for 24 hr. Then, 1% (w/v) aqueous suspensions of calcium hydroxide [$Ca(OH)_2$], nanohydroxyapatite (nHA; < 200 nm), and β-tricalcium phosphate (βTCP) were incorporated (separately) into chitosan solution by dripping at a 1:2 ratio and under 1000 rpm stirring for 5 min. The prepared solutions (CH, CH-Ca, CH-nHA, and CH-βTCP) were added to acrylic molds and subjected to a phase-separation process at low temperatures with gradual freezing in a -20ºC freezer for 4 hr, overnight at -80ºC, followed by immersion in liquid nitrogen at -198ºC for 30 min. Afterward, the samples were freeze-dried at -84ºC for 24 hr (FreeZone, Labconco Corporation, Kansas City, MO, USA). Scaffolds 6 mm in diameter and 3 mm thick were obtained by means of a biopsy punch (Kolplast ci LTDA.; Itupeva, SP, Brazil). The samples were then subjected to the cross-linking process in 25% glutaraldehyde vapor for 6 hr. This protocol can modulate degradability while maintaining the porous architecture of the material after immersion in a liquid medium and does not cause cytotoxicity (Soares et al., 2020).

2.1.2 | *Biomineralization procedure in SBF*

The SBF solution was prepared as described by Kokubo and Takadama (2006), with an inorganic ion concentration 1.5 times that of human blood plasma, previously established by Wei and Ma (2006). Before incubation, the scaffolds were stabilized by immersion in 70% ethanol, followed by vacuum incubation for 30 min for the elimination of bubbles. Then, they were washed in phosphate-buffered saline (PBS; pH 7.4, Gibco®, Invitrogen™, Carlsbad, CA, USA). The scaffolds from each group were immersed in SBF solution and incubated for 5 days at 37ºC under 100 rpm agitation, and the solution was renewed every 48 hr. The scaffolds were removed from the solution and immersed in deionized water for 24 hr for the removal of insoluble inorganic ions (Zhang & Ma, 2004), then gently dried with an absorbent paper towel and frozen at -20ºC. They were then freeze-dried at -84ºC overnight. The groups subjected to biomineralization were named CH_{SBF}, $CH\text{-}Ca_{SBF}$, $CH\text{-}nHA_{SBF}$, and $CH\text{-}\beta TCP_{SBF}$. The procedure for scaffold manufacturing is demonstrated in Figure 1a-1c.

2.1.3 | *Characterization of morphology and porosity*

The surface topography of the scaffolds subjected or not to incubation in SBF was evaluated under a Scanning Electron Microscope (SEM; PSEM eXpress, Aspex

Corporation, Delmont, PA, USA). For this, the samples were positioned in stubs with carbon tape and coated with gold. The analyses were performed at an accelerating voltage of 15 kV with magnifications from 100x to 2500x. The porosity of the scaffolds (%) and pore diameter (µm; 115 units/sample) were calculated (n = 3) by means of ImageJ software (National Institutes of Health, Bethesda, MD, USA),

2.1.4 | *Chemical structure characterization*

The chemical structure was evaluated by Fourier Transform Infrared Spectroscopy (FTIR) in the Attenuated Total Reflectance (ATR) mode by means of Shimadzu FT-IR-8300 equipment (Shimadzu Corporation, Kyoto, Honshu, Japan). Three samples from each group were placed in a standard position by means of a low-pressure press (Shimadzu Corporation) on the diamond crystal ATR (Smart Miracle™, Pike Technologies, Madison, WI, USA). Three readings were taken with an average of 32 scans between 4500 and 400 cm^{-1} and a resolution of 4 cm^{-1} at room temperature.

2.1.5 | *Degree of degradability of scaffolds*

The degree of degradability (DG) of the materials incubated or not in SBF was evaluated by calculation of the mass loss over 28 days (n = 6) by the wet-weight technique. The samples were incubated in 500 µL of PBS at 37°C for 1 hr. Subsequently, they were dried with absorbent paper for 15 min, and the initial wet weight (baseline) was measured on a precision electronic balance (MG214Ai 220g; Bel Engineering, Monza, MB, Italy). The samples were then incubated for 28 days at 37°C, with the PBS solution being renewed weekly. The weight was measured again after 1, 7, 14, 21, and 28 days of incubation. The DG was determined according to the formula DG (%) = ((Pf-Pi)/Pi)) x 100, where Pi represents the initial wet weight and Pf the final wet weight after immersion in PBS.

2.1.6 | *Calcium release*

This analysis was performed by immersion of the samples in 200 µL of ultrapure distilled water (Life Technologies, Carlsbad, CA, USA), pH 7.2, and at 37ºC for 1, 7, 14, and 21 days (n = 3). At each time-point, an aliquot was removed for reading by reaction with the o-cresolphthalein complexone substrate (Labtest Diagnóstica S.A., Lagoa Santa, MG, Brazil). Absorbance was quantified at 570 nm (Synergy Mx; BioTek Instruments,

Winooski, VT, USA), and the data were converted into concentration (mg/dL) on a standard curve.

2.2 | Biological analysis in vitro

2.2.1 | *Culture of Human Dental Pulp Cells (HDPCs)*

HDPCs were obtained as previously described by Soares et al. (2018) after ethics approval (Human Research Ethics Committee - Bauru School of Dentistry, University of São Paulo - USP - CAAE 26153119.6.0000.5417). Briefly, the pulp tissue was collected from three sound third molars (one donor; 20 years old) and subjected to enzymatic disaggregation in collagenase type I solution (3 mg/mL, Sigma-Aldrich). Following an adhesion phase of 3 hr, the cells were subcultivated in fresh complete α-MEM (alpha Minimum Essential Medium, supplemented with 10% fetal bovine serum [FBS], L-glutamine, and 1% penicillin-streptomycin; GIBCO, Invitrogen, Carlsbad, CA, USA). Cells at passages 4-6 were used in this study.

2.2.2 | *Direct contact analysis*

The scaffolds were sterilized in 70% ethanol for 30 min, followed by the removal of internal bubbles in a vacuum. Then, samples were positioned in 48-well plates containing 500 µL of PBS. Residual ethanol was removed with three 15-minute baths in PBS, followed by overnight incubation in complete α-MEM culture medium (GIBCO®, Invitrogen) at 37°C and 5% CO_2. The medium was gently aspirated from the scaffolds, and cells (1 x 10^5 cells) were seeded in a 5-µL drop over the samples to avoid cell spillage onto the culture plate (Figure 1d). The cell/scaffold constructs were incubated at 37ºC and 5% CO_2 for 30 min to allow for initial adhesion. Then, a 500-µL quantity of complete α-MEM culture medium was added, followed by 24-hour cultivation. Thereafter, the constructs were cultivated in complete α-MEM for cell viability analysis, or in an osteogenic medium (complete α-MEM supplemented with 50 mM ascorbic acid; 10 mM β-glycerophosphate; Sigma-Aldrich) for the alkaline phosphatase (ALP activity) and mineralized matrix deposition (Alizarin Red) assays. The analyses described below were performed with two independent experiments to ensure reproducibility of the results.

(a) Cell viability: After 1, 3, 7, and 14 days of culture, the scaffolds (n = 2) were washed in PBS and incubated with culture medium supplemented with Calcein AM and Ethyl Homodimer-1 (Live/Dead® Viability/Cytotoxicity Kit; Invitrogen, Carlsbad, CA, USA) at a concentration of 1:1000 for 15 min. Then, the presence of viable and dead cells on

scaffolds was analyzed under a fluorescence microscope (FLoid, Life Technologies, Carlsbad, CA, USA).

(b) Quantification of cell viability (Alamar Blue): The Alamar Blue assay was performed after 1, 7, and 14 days of culture to quantify cell viability in the different periods, indirectly measuring cell proliferation. In each analysis, the constructs (n = 6) were incubated for 3 hr at 37ºC and 5% CO_2 with the Alamar Blue® reagent (Life Technologies, Carlsbad, CA, USA) diluted in α-MEM without serum (1:10). After this period, the supernatant was transferred to 96-well plates and analyzed in a fluorescence reader (540 nm excitation - 590 nm emission; Synergy Mx; BioTek Instruments, Winooski, VT, USA). The data were normalized based on the control group (CH), and the viability of the control group was considered as 100% in each period.

(c) ALP activity: ALP activity was measured at 7 and 14 days of culture by means of the Alkaline Phosphatase kit (Labtest Diagnóstica S.A.; Lagoa Santa, MG, Brazil). The scaffolds (n = 6) were washed with PBS, transferred to 1.5-mL tubes, and incubated in 0.1% sodium lauryl sulfate solution for 40 min. Then, the samples were cut and macerated, and 100 µL of buffer and 10 µL of substrate were added to each tube, followed by incubation for 15 min at 37ºC. Subsequently, a 400-µL quantity of color reagent was added to each tube, which was then centrifuged at 12,000 rpm for 5 min. A 200-µL aliquot of the supernatant from each tube was transferred to a 96-well plate, and the absorbance was read at 590 nm (Synergy Mx; BioTek Instruments, Winooski, VT, USA). The data were obtained according to a standard curve and normalized by the total protein concentration method (Lowry/Folin-Ciocalteu method; Soares et al., 2020). The results were normalized by the volume (mm^3) of the scaffolds. The CH group was considered as 100% of ALP activity.

(d) Mineralized matrix deposition (Alizarin Red): After 14 and 21 days of culture, the scaffolds (n = 6) were washed with PBS and fixed in 70% ethanol at 4ºC overnight. Then, they were washed in PBS and incubated for 20 min in Alizarin Red solution (40 mM, pH 4.2; Sigma-Aldrich). The scaffolds were washed with deionized water to remove excess dye and transferred to 1.5-mL tubes containing 500 µL of 10% cetylpyridinium chloride solution to dissolve the deposited minerals. The tubes were centrifuged at 4000 rpm for 2 min, and a 150-µL quantity of supernatant was collected from each tube and transferred to a 96-well plate for absorbance reading at 570 nm (Synergy Mx, BioTek, Winooski, VT, USA). Cell-free scaffolds were used to eliminate the background. The results were normalized by the volume (mm^3) of each sample of scaffolds. The CH group was considered as 100% of mineralized matrix deposition.

2.2.3 | *Biological analysis of scaffolds at a distance: cell-homing applicability (indirect method)*

For evaluation of the effects of the compounds released by the samples, scaffolds incubated or not in SBF were later incubated in osteogenic medium at 37°C and 5% CO_2 for up to 21 days to obtain a conditioned medium (extracts; n = 6), which was applied to the cells every 24 hr. On the day of incubation of the scaffolds, HDPCs (1.5 x 10^3 cells) were seeded in 96-well plates and cultured in complete α-MEM at 37°C and 5% CO_2 for 24 hr. Then, the cell medium was replaced with the 24-hour extracts and renewed with the new extracts obtained daily (Figure 1d). ALP activity was measured after 7 and 14 days, and mineralized matrix deposition (Alizarin Red) at 14 and 21 days, according to the protocol described previously, except for the maceration and centrifugation steps, since measurement was performed directly on the plate where the cells were seeded.

2.3 | Statistical analysis

Shapiro-Wilk ($p>0.05$) and Levene tests ($p>0.05$) were performed to evaluate data normality and homoscedasticity, respectively. Data from independent experiments were compiled and analyzed by one- or two-way ANOVA complemented by Tukey's or Dunnett´s test for observation of the significant differences between the study groups ($p < .05$ = statistically significant).

3 | RESULTS

3.1 | Physical/chemical characterization of the scaffolds

3.1.1 | *Scaffold architecture*

The SEM images of scaffolds incubated or not in SBF and subjected to the lyophilization procedure are presented in Figure 2. CH presented a disorganized porous architecture, whereas the addition of mineral phases to CH was responsible for creating larger pores. This effect was more evident for CH-Ca and CH-nHA, in which an organized macro-pore network was observed, with round pores. CH-βTCP presented a less organized architecture but with larger pores than CH. Incubation in SBF altered CH scaffold architecture, in which it was possible to observe the presence of a discrete and almost imperceptible coating on the external surface. CH-Ca_{SBF} retained the macro-porous

architecture, and disperse mineral-like deposits could be observed on its structure. Nevertheless, CH-nHA$_{SBF}$ and CH-βTCP$_{SBF}$ presented a disorganized architecture and the presence of large mineral deposits on their surfaces, which was more evident for CH-nHA$_{SBF}$.

3.1.2 | *Chemical composition*

Figure 3a shows the FTIR spectra of the reference spectra of $Ca(OH)_2$, nHA, and βTCP, and for the materials after the incorporation of $Ca(OH)_2$, nHA, and βTCP into chitosan. The $Ca(OH)_2$ spectrum showed characteristic bands at 3640 cm^{-1} and a strong band at 500 cm^{-1}, corresponding to O─H and Ca-O stretching vibrations, respectively. The reference spectra of the nHA and βTCP mineral phases showed characteristic strong bands, easily distinguished and assigned to the PO_4^{-3} groups, referring to stretching and angular vibrations. The bands at 1102 cm^{-1} and 1040 cm^{-1} were assigned to asymmetric -P-O stretching components, triply degenerate. The band at 964 cm^{-1} was assigned to symmetric -P-O stretching modes. The components of the angular -O-P-O- triply degenerate vibration mode were assigned bands at 601 cm^{-1} and 570 cm^{-1} for HA and 601-588 cm^{-1} and 540 cm^{-1} for βTCP. The angular -O-P-O- double-degenerate modes of vibration were in the range 462-474 cm^{-1}. The weak band could appear at 875 cm^{-1}, referring to HPO_4^{-2}. The band at 3400 cm^{-1} refers to the symmetric -OH stretching of the structure (Ślósarczyk, Paluszkiewicz, Gawlicki, & Paszkiewicz, 1997). The bands at 3560 cm^{-1} and 632 cm^1, corresponding to the -OH structure, were present in apatite (HA) and absent in β-TCP precursors.

It was possible to observe the characteristic absorption bands for the CH scaffold (Jeon, & Höll, 2003; Amaral, Granja, & Barbosa, 2005; Yuan, Shah, Hein, & Misra, 2010; Zeng et al., 2011; Thomas et al., 2018). The changes in the wavelengths and intensities of the characteristic bands indicated the chemical changes in the structures of the CH-Ca, CH-nHA, and CH-βTCP scaffolds as a function of the addition of the mineral phases. It was possible to notice, through the extended region, changes in the 1640, 1606, 1550, 1443, 1413, 1381, 1315, and 1066 cm^{-1} bands relative to the -N-H stretching, amine, and amide vibrations (-NH2, -NHCO, -C-N) and C-O stretching, indicating the involvement of the amino and C-O groups in the complexation with ions from the added mineral phases, such as calcium or phosphate groupings, as a function of the changes in the absorption bands at 1066, 1028, and 655 cm^{-1}.

Figure 3b-3e presents the comparison of FTIR spectra of the scaffolds of the CH, CH-Ca, CH-nHA, and CH-βTCP groups, before and after immersion in SBF solution, for evaluation of the biomineralization characteristics indicative of hydroxyapatite

deposition. As mentioned previously, the reference spectrum of HA shows that characteristic bands for PO_4^{-3} groups could be observed at 472, 566, 601, 960, 1027, and 1100 cm^{-1}. The bands corresponding to the structural -OH groups of apatite were assigned at 630 cm^{-1} and 3560 cm^{-1} (Cardenas-Triviño & Carrasco-Garcia, 2019). It was possible to notice differences in the main amide I, II, and III bands, with significant variations in intensities and positions. There was a significant change in the 1120-975 cm^{-1} regions, referring to the stretching of -C-O groups of the chitosan structure. Another significant change occurred in the 620-558 cm^{-1} region, where prominent new absorption bands were noted located at 1022, 601, and 559 cm^{-1}, consistent with the prominent absorption bands of hydroxyapatite, referring to the phosphate groups present in the structure (Danylchenko, Kalinkevich, & Pogorelov, 2009).

3.1.3 | *Pore size and porosity degree*

Analysis of SEM images indicated that CH-Ca and CH-βTCP featured the largest pore diameters, whereas the other groups presented similar pore sizes in comparison with CH (Figure 4a). Nevertheless, calculation of the degrees of porosity (Figure 4b) indicated that all mineral phases increased the percentage of porosity statistically significantly in comparison with CH, with CH-Ca and CH-Ca_{SBF} showing the highest values, followed by CH-βTCP and CH-nHA. In contrast, SBF treatment intensely reduced the degrees of porosity of CH-nHA_{SBF} and CH-βTCP_{SBF}.

3.1.4 | *Calcium release and degradation profile*

The cumulative calcium (Ca^{2+}) release profile of the scaffolds is shown in Figure 4c. The CH-nHA and CH-βTCP scaffolds subjected or not to SBF treatment had the highest release at all time-points, with a cumulative profile throughout 21 days. CH-Ca had a peak of Ca^{2+} release at 7 days that was not detected on CH-Ca_{SBF}. Regarding the degradation profile (Figure 4d), CH showed no alteration in wet mass throughout the 28-day period. The addition of mineral phases led to a high degradation rate of the scaffolds when immersed in a neutral aqueous medium starting at 7 days for CH-βTCP and CH-βTCP_{SBF}, and at 14 days for CH-Ca, CH-nHA, and CH-nHA_{SBF}. Incubation of CH and CH-Ca in SBF resulted in no difference in wet weight over time when compared with their respective baselines.

3.2 | In vitro biological characterization

3.2.1 | *Direct contact assay*

For all experimental groups, the cells remained viable and were able to proliferate over time, as demonstrated by Live/Dead and Alamar Blue assays (Figure 5), indicating that all formulations were cytocompatible. It was possible to observe, in Live/Dead images (Figure 5a), that CH-Ca and CH-nHA cells spread throughout the scaffold structure at 14 days, presenting a stretched cytoplasm, where cells in the CH group were dispersed on the material structure. Cells in CH-βTCP had a tendency to form agglomerates. The stretched cell architecture could also be noted on CH-Ca_{SBF} at the 14-day period; nevertheless, cell agglomerates were observed for the CH-nHA_{SBF} and CH-βTCP_{SBF} groups. It was also possible to observe a higher cell density on CH-Ca, CHnHA, and CH-βTCP formulations, subjected or not to SBF treatment, in comparison with that of CH and CH_{SBF} groups, starting at 7 days. The Alamar Blue assay (Figure 5b) detected increased cell viability values for mineral-rich SBF-treated groups at 7 days, and for all experimental groups at 14 days, in comparison with those of the CH group. A considerable increase in viability was observed at 7 and 14 days compared with the CH group for the formulations incubated in SBF, especially in the CH-nHA_{SBF} and CH-βTCP_{SBF} groups. There was an increase in ALP activity for all groups over time (Figure 5c). The addition of mineral phases did not affect the ALP activity of the groups compared with the CH control. Incubation in SBF increased ALP activity for all mineral-rich SBF-treated groups in both periods of analysis. The positive effect of mineral phase incorporation in association with SBF treatment was also detected in the Alizarin Red assay (Figure 5d). Incorporation of a mineral phase alone promoted significant increases in mineralized matrix deposition at 14 days in comparison with the CH group by 1.9 to 2.4 times; nevertheless, association with SBF treatment led to increases of 9.8, 18.9, and 8.4 times in mineralized matrix deposition for the CH-$Ca_{SBF,}$ CH-nHA_{SBF}, and CH-βTCP_{SBF} groups, respectively, in comparison with CH.

3.2.2 | *Effects of conditioned medium*

In evaluation of the effects of the compounds released by the samples over HDPC activity, it was possible to observe higher ALP activity at 14 days for all groups after the addition of the mineral phases when compared with the CH control (Figure 6a). Incubation in SBF increased the ALP activity in all groups at 14 days compared with the CH control, and also with respective formulations with no SBF treatment. Regarding mineralized matrix deposition (Figure 6b), the addition of mineral phases led to increased

deposition in the CH-Ca and CH-β-TCP groups at 21 days compared with the CH control group. Incubation in SBF increased deposition at 21 days for all groups compared with the CH control group.

4 | DISCUSSION

Currently, there are increasing efforts to modulate tissue regeneration by the development of biomaterials that can adapt to the biological microenvironment where they are inserted, inducing specific cellular responses that optimize the repair process (Ahmed, Abouauf, AbuBakr, Dörfer, & El-Sayed, 2020; Bottino, Pankajakshan, & Nör, 2017). In the present study, we proposed the fabrication of chitosan scaffolds associated with different mineral phases and subjected to a biomineralization process in SBF, to create biomimetic scaffolds for application in direct pulp-capping. Phase-separation is a simple method to form chitosan scaffolds by segregating the polymeric phase during freezing, followed by ice elimination via freeze-drying. However, this technique provides no control over the degree of porosity (Madihally & Matthew, 1999; Zhu, Wan, Zhang, Yin, & Cheng, 2014; Aranaz et al., 2017). Therefore, in this study we applied a manufacturing method previously developed by our group (Soares et al., 2020), in which a $Ca(OH)_2$ suspension is added to the CH solution under stirring, at a 1:2 ratio, creating highly porous scaffolds with increased and organized pores in comparison with pure chitosan scaffolds. The other mineral phases used in this study, βTCP and nHA, were incorporated in the same way and at the same proportions, and the effects of these incorporations were analyzed.

According to our results, $Ca(OH)_2$, nHA, and βTCP were capable of modulating the porous architecture of chitosan scaffolds, increasing pore size and overall porosity. Nevertheless, only CH-Ca and CH-nHA had a round and well-distributed porous network, with an interconnected porous structure. Incorporation of βTCP created an open pore structure, albeit with a disorganized architecture. CH-Ca had the highest pore size and porosity degree, followed by CH-βTCP and CH-nHA. The mechanisms related to porous architecture mediated by $Ca(OH)_2$ were a consequence of CO_2 release during the slow and gradual freezing process, resulting in bubbles that underwent expansion within the polymeric mesh (bubbling effect), creating the round and interconnected pores. The incorporation of $Ca(OH)_2$ acted as the CO_2 source upon carbonation and reactions with acetic acid, increasing the pore diameter and total porosity compared with those of plain chitosan scaffolds (Soares et al., 2020). Therefore, based on our results, we believe that βTCP and nHA also promoted a bubbling effect upon incorporation into chitosan solution,

leading to pore enlargement as observed by SEM images. Kim et al. (2015) obtained similar results by incorporating alginate-nHA dispersion into a 4% chitosan solution in a 1% acetic aqueous solution, avoiding the occurrence of mineral agglomerates. A clear chitosan/alginate/nHA solution was obtained, which was then gradually frozen from 4°C to -20°C, and freeze-dried at -89°C. A chitosan scaffold showing a homogeneous round pore network, with pore size varying from 100 to 400 μm, and porosity higher than 80%, was achieved, whereas the plain chitosan solution resulted in a lamellar pore network. Other researchers also demonstrated that an acid-base reaction of citric acid with $NaHCO_3$ produced CO_2 bubbles in $CaCO_3$ scaffolds, giving rise to an organized macro-porous architecture (Chen et al., 2012; Thein-Han, & Xu, 2013; Chen, Thein-Han, Weir, Chen, & Xu, 2014).

Besides modulating overall scaffold architecture, the $Ca(OH)_2$ mineral-induced bubbling effect also led to calcium (Ca^{2+}) complexation to chitosan, creating the CH-Ca scaffold, which also acted as a calcium-release system capable of increasing the odontogenic potential of human dental pulp cells by increasing the deposition of mineralized tissue (Soares et al., 2020). The FTIR analysis of current formulations confirmed that Ca^{2+} was indeed complexed to chitosan on CH-Ca, and also demonstrated that Ca^{2+} and PO_4^{3-} were incorporated into chitosan on CH-βTCP and CH-nHA. Upon incubation of an apatite source in acid solution, the dissolution process occurred, in which H+ and anions of acid from the bulk solution promoted the release of Ca^{2+} and PO_4^{3-} from mineral surfaces (Dorozhkin, 2012). These ions were susceptible to chemical interaction in the amino, hydroxyl, and acetyl groups of the chitosan molecule (Pestov & Bratskaya, 2016; Shakir et al., 2015; Kar, Kaur, & Thirugnanam, 2016; Keikhaei, Mohammadalizadeh, Karbasi, & Salimi, 2019). Our results also suggested these interactions. The changes regarding -N-H stretching, amine and amide vibrations, and C-O stretching demonstrate the involvement of these groups in the complexation of the Ca^{2+} and PO_4^{3-} ions present in the added suspensions.

In addition to the incorporation of $Ca(OH)_2$, βTCP, and nHA as bioactive mineral phases, in this study we used a biomimetic mineralization technique for manufacturing the biomaterials. This technique is based on the incubation of the samples in SBF, a solution with ions in concentrations similar to those found in human blood plasma. Rich in Ca^{2+} and PO_4^3, this fluid can promote the formation of calcium phosphate (Ca-P) crystalline structures similar to the apatite found in native bone and has been used to improve the bone-regeneration properties of scaffolds by mimicking the natural bone surface, promoting an ideal environment for osteogenesis, and increasing the structural

stability of the scaffold (Xin, Leng, Chen, & Zhang, 2005; Castro, Tan, Shen, & Zhang, 2016; Shin, Acri, Geary, & Salem, 2017).

SBF-mediated mineralization occurs in a series of events, beginning with the high concentrations of Ca^{2+} and PO_4^{3-} contained in the solution that form pre-nucleation crystals. The amorphous solids are then attracted to the polar surface groups of the substrate. The apatite crystals are deposited, and the formed apatite becomes a nucleation site, allowing more crystals to grow continuously (Shin, Acri, Geary, & Salem, 2017). Incubation parameters in SBF have undergone significant changes since its first formulation, to accelerate the deposition and coating of biomaterials. Thus, studies have evaluated factors such as concentration and composition of the solution, aiming to improve the surface-coating characteristics (Yuan, Mak, & Li, 2001; Wei & Ma, 2006; Guastaldi & Aparecida, 2010). A higher ionic concentration of the SBF solution facilitates apatite formation. In a study by Zhang and Ma (2004), incubation of polymeric scaffolds in SBF at a 1.5-fold concentration was responsible for higher apatite deposition compared with the conventional concentration, indicating that increasing the ionic concentration may be a practical way to facilitate apatite nucleation and growth, probably due to the higher availability of Ca^{2+} and PO_4^{3-} to be precipitated. Therefore, we selected this SBF concentration to promote Ca-P covering on our macro-porous scaffolds, which was confirmed by FTIR as indicative of hydroxyapatite, by the intense absorption bands corresponding to the phosphate groups observed in SBF-treated samples.

The scaffolds from the CH-nHA group subjected to biomineralization showed intense mineral coverage when compared with the other groups. This also occurred in a previous study, in which Wei and Ma (2006) demonstrated that pre-incorporation of nHA (even in low proportions) into poly(L-lactic acid) (PLLA)-based polymeric scaffolds induced greater apatite formation when in SBF compared with a pure polymeric scaffold. This can be explained by the higher ionic availability provided by the presence of nHA in the scaffold, which may have facilitated the formation of nucleation sites and allowed for greater crystal growth. This effect was also detected for CH-βTCP, since large mineral structures were detected on scaffold surfaces, whereas CH and CH-Ca showed only a slight, almost imperceptible mineral deposition. Therefore, Ca-P seems to play an important role as pre-nucleation for biomineralization to occur. Nevertheless, the porous structure of CH-nHA and CH-βTCP was intensely disrupted, which affected cell infiltration and spread throughout the scaffold structure. Only the CH-Ca scaffold subjected to SBF treatment maintained the macro-porous and interconnected network, as observed by SEM images, denoting the more stable and predictable architecture provided by the bubbling effect mediated by $Ca(OH)_2$.

An important parameter in tissue engineering is scaffold biodegradability, because, as a temporary structure, the scaffold must be replaced by new tissue (Murphy, Kohn, & Mooney, 2000). Therefore, the biomaterial must have a controlled rate of biodegradability, which must be consistent with the rate of new tissue formation (Ribeiro, Vieira, Melo, Araújo, & Lima, 2017; Islam, Shahruzzaman, Biswas, Nurus Sakib, & Rashid, 2020). In this study, the addition of mineral phases led to a higher scaffold degradation rate when immersed in a neutral aqueous medium. Overall, biomineralization was responsible for a slight increase in the percentage of this degradation, except for the CH-Ca_{SBF} group. However, even with the loss of mass, the scaffolds of all groups remained viable for cell interaction throughout the 21 days of analysis in vitro, which was enough time to allow for cell differentiation and deposition of the mineralized matrix by the HDPCs, as proven by the results of the biological analyses that will be discussed further. In our previous in vivo study using CH-Ca in rat calvaria, the scaffold remained stable for mineralized tissue regeneration after the 30-day period, as detected by histological sections (Soares et al., 2021).

From a biological perspective, the incorporation of mineral phases into the chitosan scaffold is proposed to increase bioactivity and accelerate the formation of the mineralized matrix. In our first proposal, $Ca(OH)_2$ was selected, since it is the most common cement used for direct pulp-capping. Therefore, we were able to demonstrate that it was possible to create a bioactive matrix with a porous structure using this inexpensive mineral phase, capable of acting as a controlled calcium-release system. Using this tissue-engineering strategy, we were able to propose a 3D matrix capable of modulating tissue regeneration by stimulating resident pulp cells and boosting odontoblastic differentiation and mineralized matrix deposition (Soares et al., 2020). More recently, we also demonstrated that CH-Ca had a chemotactic potential with dental pulp cells, using an artificial pulp chamber model in vitro, in which we were able to demonstrate that cells migrated from a 3D culture in intimate contact with cell-free CH-Ca, infiltrating its porous network and expressing odontogenic-related proteins. This porous material also improved new bone deposition toward the centers of critical-sized defects in rat calvaria in vivo, demonstrating its potential as an inductive cell-homing platform for mineralized tissue regeneration, such as bone and dentin (Soares et al., 2021). These homing effects were related to Ca^{2+} released by biomaterials, resulting in an influx of Ca^{2+} in the intracellular environment through the activation of Ca^{2+} channels, which would increase the expression of genes related to odontogenic differentiation (An, Gao, Ling, Wei, & Xiao, 2012; Gandolfi et al., 2015; Kuzmenka et al., 2020). An et al. (2012) investigated the effects of different Ca^{2+} concentrations on the growth and

odontogenic differentiation of HDPCs, concluding that the odontogenic properties of these cells can be influenced by the Ca^{2+} content present in the culture medium, and that, therefore, it is important to optimize the release of these ions for a better clinical outcome in pulp-capping materials. Chitosan-based vehicles targeting sustained Ca^{2+} release have been developed and have demonstrated an adequate calcium-release profile in addition to cytocompatibility (Farhadian, Godiny, Moradi, Azandaryani, & Shahlaei, 2018; Flores-Arriaga et al., 2019).

In the current study, we went a step further to demonstrate if traditional Ca-P sources, commonly used for bone regeneration, would result in better effects as bioactive tools in our manufacturing method. Due to the excellent results of βTCP and HA in bone regeneration, these mineral phases have also been proposed for dentin regeneration, with exciting results. AbdulQader et al. (2015) investigated the proliferation and differentiation of HDPCs under the effects of extracts obtained from scaffolds with different proportions of HA and β-TCP. Cells cultured with the extracts from scaffolds in the β-TCP at a 20/80 HA ratio showed high ALP activity and positive regulation of the expression levels of bone sialoprotein (BSP), dentin matrix protein-1 (DMP-1), and dentin sialophosphoprotein (DSPP), genes associated with the differentiation and maturation process of odontoblasts. In another in vitro study, immortalized HDPCs exhibited odontogenic differentiation and DSPP expression when combined with a scaffold of βTCP and bone morphogenetic protein (BMP2) (Li et al., 2020). Recently, Guerrero-Gironés et al. (2021) evaluated the effect of a scaffold containing βTCP, HA, and collagen (C) on the vital pulp of rat molars, comparing it with mineral trioxide aggregate (MTA), and demonstrated superior results on mineralized barrier deposition. Cao et al. (2020) analyzed two types of 3D-printed scaffolds, one based on poly(lactic acid-co-glycolic acid) in association with βTCP (3D-PLGA/β-TCP) and another based on βTCP (3D-TCP). Both formulations increased the adhesion and proliferation of HDPCs, and promoted odontogenic differentiation.

Therefore, we performed two in vitro assays to observe the biological activities of current formulations, by cultivating HDPCs directly on the scaffolds (direct contact) and exposing them to their extracts (remote). It was possible to observe that all formulations were cytocompatible and allowed cells to proliferate through time within the scaffold structure. An interesting find referred to cell spread throughout scaffold structure at the 14-day period, observed by the Live/Dead assay. This effect was more evident for CH-Ca and CH-nHA, which featured a round and interconnected macro-porous network. The macro-porous architecture of CH-βTCP resulted in cell agglomerates, but it was also possible to observe an interconnection among the clusters, which was not detected in the CH group. Following SBF treatment, we detected a disruption of the porous

architecture of CH-nHA$_{SBF}$ and CH-βTCP$_{SBF}$ due to intense Ca-P deposition, which resulted in large cell agglomerates. Only CH-Ca$_{SBF}$ retained the macro-porous architecture, allowing for a better cell spread. Since the CH scaffold had a lower degree of porosity and disconnected porous architecture, the cells appeared dispersed on its surface. A positive effect of SBF treatment on cell proliferation was detected, since the Alamar Blue assay revealed a considerable increase in cell metabolism at 7 and 14 days for the groups containing mineral phases and incubated in SBF compared with the group with pure CH (control). According to the literature, this could be explained due to the formation of the Ca-P layer on the surface, promoting greater cell adhesion between the material and the cells by increasing surface roughness, surface area, and focal adhesion points (Boone et al., 1989; Castro, Tan, Shen, & Zhang, 2016).

Regarding odontogenic differentiation, it was possible to detect that $Ca(OH)_2$, nHA, and βTCP featured similar positive effects on ALP activity and mineralized matrix deposition by the cells seeded onto scaffold structures and cultivated with conditioned medium. This bioactive effect was significantly improved by SBF treatment. An intense increase in mineralized matrix deposition could be observed for the cells in direct contact with these biomineralized scaffolds. This effect was more prominent at the 21-day time-point, with CH-nHA$_{SBF}$ featuring the highest values, increasing by 18.9 times the mineralized matrix deposited by the cells. CH-Ca$_{SBF}$ and CH-βTCP$_{SBF}$ also had stunning results, up-regulating mineralized matrix deposition by 9.8 and 8.4 times, respectively. The mineral-containing scaffolds not treated with SBF led to increased mineralized matrix deposition by 1.9 to 2.4 times. For cells cultured with the components continuously released by the scaffolds, this mineral-induced effect was similar among mineral-containing scaffold formulations (up to 1.6 times), regardless of SBF treatment.

Other studies have shown similar results, indicating that incubation in SBF has the potential to increase cell viability. A collagen scaffold, subjected to HA coating through SBF immersion, demonstrated excellent biological performance in vitro, with potential for use in bone tissue engineering (Al-Munajjed et al., 2009). Castro et al. (2016) developed porous scaffolds 3D-printed from filaments of a polyurethane-based elastomeric composite. The material was incubated in SBF for different periods, resulting in adequate nucleation of hydroxyapatite, which was responsible for increasing nanoscale surface roughness without changing the structure of the material. The nucleation of hydroxyapatite facilitated cell adhesion and spreading within the first 24 hr; differentiation was also increased, and there was an increase in the deposition of the mineralized matrix when compared with that in the control group, without biomineralization.

Therefore, the addition of mineral phases and the biomineralization coating method proposed in this investigation appear to be promising approaches capable of increasing the bioactivity of chitosan-based scaffolds for use in dentin regeneration. Nevertheless, it is important to note that only $Ca(OH)_2$ and nHA were capable of promoting an adequate mineral-induced bubbling effect on chitosan scaffolds, resulting in a large, round, well-distributed, and interconnected porous network throughout the scaffold structure. These compositions had a bioactive effect, positively modulating the odontoblastic differentiation of HDPCs. Nevertheless, the biomineralization technique resulted in intense mineral deposits on nHA surfaces, disrupting the porous architecture and interfering with cell spread. Collective results suggest that the biomineralized CH-Ca formulation appears to be an interesting biomaterial for boosting dental pulp cell mineralization phenotypes, while maintaining the macro-porous architecture that is crucial for a cell-homing strategy. The significant advantage of this formulation is its lower cost relative to that of the other tested Ca-P mineral phase, and its simple fabrication process. Therefore, further studies are necessary to prove its potential as a designed scaffold applicable for dentin tissue engineering.

5 | CONCLUSIONS

This study demonstrated that the incorporation of proposed mineral phases as suspensions into chitosan solutions following a specific phase-separation route promotes a mineral-induced bubbling effect, modulating porous scaffold architecture, chemical composition, and degree of degradability, creating interesting porous and bioactive scaffolds for mineralized tissue regeneration. Also, biomineralization with SBF improved the bioactive potential of these formulations, regardless of the disruption of porous architecture in selected formulations. Overall, the CH-Ca scaffold subjected to biomineralization was the sole composition capable of maintaining the macro-porous architecture, being capable of boosting the proliferation and mineralizing phenotypes of dental pulp cells seeded onto its structure, and at a distance, similarly to traditional Ca-P phases, presenting the potential for the development of low-cost cell-free strategies for dentin tissue engineering.

REFERENCES

1. da Rosa, W., Cocco, A. R., Silva, T., Mesquita, L. C., Galarça, A. D., Silva, A., & Piva, E. (2018). Current trends and future perspectives of dental pulp capping

materials: A systematic review. *Journal of biomedical materials research. Part B, Applied biomaterials*, *106*(3), 1358–1368. https://doi.org/10.1002/jbm.b.33934

2. Zaen El-Din, A. M., Hamama, H. H., Abo El-Elaa, M. A., Grawish, M. E., Mahmoud, S. H., & Neelakantan, P. (2020). The effect of four materials on direct pulp capping: An animal study. *Australian endodontic journal: the journal of the Australian Society of Endodontology Inc*, *46*(2), 249–256. https://doi.org/10.1111/aej.12400

3. Widbiller, M., & Schmalz, G. (2021). Endodontic regeneration: hard shell, soft core. *Odontology*, *109*(2), 303–312. https://doi.org/10.1007/s10266-020-00573-1

4. Soares, D. G., Bordini, E., Swanson, W. B., de Souza Costa, C. A., & Bottino, M. C. (2021). Platform technologies for regenerative endodontics from multifunctional biomaterials to tooth-on-a-chip strategies. *Clinical oral investigations*, *25*(8), 4749–4779. https://doi.org/10.1007/s00784-021-04013-4

5. Piva, E., Silva, A. F., & Nör, J. E. (2014). Functionalized scaffolds to control dental pulp stem cell fate. *Journal of endodontics*, *40*(4 Suppl), S33–S40. https://doi.org/10.1016/j.joen.2014.01.013

6. Galler, K. M., Eidt, A., & Schmalz, G. (2014). Cell-free approaches for dental pulp tissue engineering. *Journal of endodontics*, *40*(4 Suppl), S41–S45. https://doi.org/10.1016/j.joen.2014.01.014

7. Soares, D. G., Zhang, Z., Mohamed, F., Eyster, T. W., de Souza Costa, C. A., & Ma, P. X. (2018). Simvastatin and nanofibrous poly(l-lactic acid) scaffolds to promote the odontogenic potential of dental pulp cells in an inflammatory environment. *Acta biomaterialia*, *68*, 190–203. https://doi.org/10.1016/j.actbio.2017.12.037 (a)

8. Li, F., Liu, X., Zhao, S., Wu, H., & Xu, H. H. (2014). Porous chitosan bilayer membrane containing TGF-β1 loaded microspheres for pulp capping and reparative dentin formation in a dog model. *Dental materials : official publication of the Academy of Dental Materials*, *30*(2), 172–181. https://doi.org/10.1016/j.dental.2013.11.005

9. Madihally, S. V., & Matthew, H. W. (1999). Porous chitosan scaffolds for tissue engineering. *Biomaterials*, *20*(12), 1133–1142. https://doi.org/10.1016/s0142-9612(99)00011-3

10. Ribeiro, J. C. V., Vieira, R. S., Melo, I. M., Araújo, V. M. A., & Lima, V. (2017). Versatility of Chitosan-Based Biomaterials and Their Use as Scaffolds for Tissue Regeneration. *The Scientific World Journal*, 2017, 25. https://doi.org/10.1155/2017/8639898

11. Islam, M. M., Shahruzzaman, M., Biswas, S., Nurus Sakib, M., & Rashid, T. U. (2020). Chitosan based bioactive materials in tissue engineering applications-A review. *Bioactive materials*, *5*(1), 164–183. https://doi.org/10.1016/j.bioactmat.2020.01.012

12. Wei, G., & Ma, P. X. (2006). Macroporous and nanofibrous polymer scaffolds and polymer/bone-like apatite composite scaffolds generated by sugar spheres. *Journal of biomedical materials research. Part A*, *78*(2), 306–315. https://doi.org/10.1002/jbm.a.30704

13. Soares, D. G., Anovazzi, G., Bordini, E., Zuta, U. O., Silva Leite, M., Basso, F. G., Hebling, J., & de Souza Costa, C. A. (2018). Biological Analysis of Simvastatin-releasing Chitosan Scaffold as a Cell-free System for Pulp-dentin Regeneration. *Journal of endodontics*, *44*(6), 971–976.e1. https://doi.org/10.1016/j.joen.2018.02.014 (b)

14. Pestov, A., & Bratskaya, S. (2016). Chitosan and Its Derivatives as Highly Efficient Polymer Ligands. *Molecules (Basel, Switzerland)*, *21*(3), 330. https://doi.org/10.3390/molecules21030330

15. Soares, D. G., Bordini, E., Cassiano, F. B., Bronze-Uhle, E. S., Pacheco, L. E., Zabeo, G., Hebling, J., Lisboa-Filho, P. N., Bottino, M. C., & de Souza Costa, C. A. (2020). Characterization of novel calcium hydroxide-mediated highly porous chitosan-calcium scaffolds for potential application in dentin tissue engineering. *Journal of biomedical materials research. Part B, Applied biomaterials*, *108*(6), 2546–2559. https://doi.org/10.1002/jbm.b.34586

16. Soares, D. G., Bordini, E., Bronze-Uhle, E. S., Cassiano, F. B., Silva, I., Gallinari, M. O., Matheus, H. R., Almeida, J. M., Cintra, L., Hebling, J., & de Souza Costa, C. A. (2021). Chitosan-Calcium-Simvastatin Scaffold as an Inductive Cell-Free Platform. *Journal of dental research*, *100*(10), 1118–1126. https://doi.org/10.1177/00220345211024207

17. GuastaldI, A. C., Aparecida, A. H. (2010). Fosfatos de cálcio de interesse biológico: importância como biomateriais, propriedades e métodos de obtenção de recobrimentos. *Quim. Nova*, 33 (6), 1352-1358. https://doi.org/10.1590/S0100-40422010000600025

18. AbdulQader, S. T., Kannan, T. P., Rahman, I. A., Ismail, H., & Mahmood, Z. (2015). Effect of different calcium phosphate scaffold ratios on odontogenic differentiation of human dental pulp cells. *Materials science & engineering. C, Materials for biological applications*, *49*, 225–233. https://doi.org/10.1016/j.msec.2014.12.070

19. Li, X., Wang, L., Su, Q., Ye, L., Zhou, X., Song, D., & Huang, D. (2020). Highly Proliferative Immortalized Human Dental Pulp Cells Retain the Odontogenic Phenotype when Combined with a Beta-Tricalcium Phosphate Scaffold and BMP2. *Stem cells international*, *2020*, 4534128. https://doi.org/10.1155/2020/4534128

20. Cao, S., Han, J., Sharma, N., Msallem, B., Jeong, W., Son, J., Kunz, C., Kang, H. W., & Thieringer, F. M. (2020). In Vitro Mechanical and Biological Properties of 3D Printed Polymer Composite and β-Tricalcium Phosphate Scaffold on Human Dental Pulp Stem Cells. *Materials (Basel, Switzerland)*, *13*(14), 3057. https://doi.org/10.3390/ma13143057

21. Guerrero-Gironés, J., Alcaina-Lorente, A., Ortiz-Ruiz, C., Ortiz-Ruiz, E., Pecci-Lloret, M. P., Ortiz-Ruiz, A. J., Rodríguez-Lozano, F. J., & Pecci-Lloret, M. R. (2021). Biocompatibility of a HA/β-TCP/C Scaffold as a Pulp-Capping Agent for Vital Pulp Treatment: An In Vivo Study in Rat Molars. *International journal of environmental research and public health*, *18*(8), 3936. https://doi.org/10.3390/ijerph18083936

22. Zhang, R., & Ma, P. X. (2004). Biomimetic polymer/apatite composite scaffolds for mineralized tissue engineering. *Macromolecular bioscience*, *4*(2), 100–111.

https://doi.org/10.1002/mabi.200300017

23. Kasten, P., Beyen, I., Niemeyer, P., Luginbühl, R., Bohner, M., & Richter, W. (2008). Porosity and pore size of beta-tricalcium phosphate scaffold can influence protein production and osteogenic differentiation of human mesenchymal stem cells: an in vitro and in vivo study. *Acta biomaterialia*, *4*(6), 1904–1915. https://doi.org/10.1016/j.actbio.2008.05.017

24. Liu, X., Holzwarth, J. M., & Ma, P. X. (2012). Functionalized synthetic biodegradable polymer scaffolds for tissue engineering. *Macromolecular bioscience*, *12*(7), 911–919. https://doi.org/10.1002/mabi.201100466

25. Kim, H. L., Jung, G. Y., Yoon, J. H., Han, J. S., Park, Y. J., Kim, D. G., Zhang, M., & Kim, D. J. (2015). Preparation and characterization of nano-sized hydroxyapatite/alginate/chitosan composite scaffolds for bone tissue engineering. *Materials science & engineering. C, Materials for biological applications*, *54*, 20–25. https://doi.org/10.1016/j.msec.2015.04.033

26. Goodarzi, H., Hashemi-Najafabadi, S., Baheiraei, N., & Bagheri, F. (2019). Preparation and Characterization of Nanocomposite Scaffolds (Collagen/β-TCP/SrO) for Bone Tissue Engineering. *Tissue engineering and regenerative medicine*, *16*(3), 237–251. https://doi.org/10.1007/s13770-019-00184-0

27. Wang, X., Lin, M., & Kang, Y. (2019). Engineering Porous β-Tricalcium Phosphate (β-TCP) Scaffolds with Multiple Channels to Promote Cell Migration, Proliferation, and Angiogenesis. *ACS applied materials & interfaces*, *11*(9), 9223–9232. https://doi.org/10.1021/acsami.8b22041

28. Hu, J., Smith, L. A., Feng, K., Liu, X., Sun, H., & Ma, P. X. (2010). Response of human embryonic stem cell-derived mesenchymal stem cells to osteogenic factors and architectures of materials during in vitro osteogenesis. *Tissue engineering. Part A*, *16*(11), 3507–3514. https://doi.org/10.1089/ten.TEA.2010.0097

29. Zhang, Z., Hu, J., & Ma, P. X. (2012). Nanofiber-based delivery of bioactive agents and stem cells to bone sites. *Advanced drug delivery reviews*, *64*(12), 1129–1141. https://doi.org/10.1016/j.addr.2012.04.008

30. Kokubo, T., & Takadama, H. (2006). How useful is SBF in predicting in vivo bone bioactivity?. *Biomaterials*, *27*(15), 2907–2915. https://doi.org/10.1016/j.biomaterials.2006.01.017

31. Murphy, W. L., Kohn, D. H., & Mooney, D. J. (2000). Growth of continuous bonelike mineral within porous poly(lactide-co-glycolide) scaffolds in vitro. *Journal of biomedical materials research*, *50*(1), 50–58. https://doi.org/10.1002/(sici)1097-4636(200004)50:1<50::aid-jbm8>3.0.co;2-f

32. Ślósarczyk, A., Paluszkiewicz, C., Gawlicki, M., & Paszkiewicz, Z. (1997). The FTIR spectroscopy and QXRD studies of calcium phosphate based materials produced from the powder precursors with different Ca/P ratios. *Ceramics International, 23*, 297-304.

33. Jeon, C., & Höll, W. H. (2003). Chemical modification of chitosan and equilibrium study for mercury ion removal. *Water research*, *37*(19), 4770–4780. https://doi.org/10.1016/S0043-1354(03)00431-7

34. Amaral, I. F., Granja, P. L., & Barbosa, M. A. (2005). Chemical modification of chitosan by phosphorylation: an XPS, FT-IR and SEM study. *Journal of biomaterials science. Polymer edition*, *16*(12), 1575–1593. https://doi.org/10.1163/156856205774576736

35. Yuan, Q., Shah, J., Hein, S., & Misra, R. D. (2010). Controlled and extended drug release behavior of chitosan-based nanoparticle carrier. *Acta biomaterialia*, *6*(3), 1140–1148. https://doi.org/10.1016/j.actbio.2009.08.027

36. Zeng, W., Huang, J., Hu, X., Xiao, W., Rong, M., Yuan, Z., & Luo, Z. (2011). Ionically cross-linked chitosan microspheres for controlled release of bioactive nerve growth factor. *International journal of pharmaceutics*, *421*(2), 283–290. https://doi.org/10.1016/j.ijpharm.2011.10.005

37. Thomas, M. S., Pillai, P. K., Faria, M., Cordeiro, N., Barud, H., Thomas, S., & Pothen, L. A. (2018). Electrospun polylactic acid-chitosan composite: a bio-based alternative for inorganic composites for advanced application. *Journal of Materials Science: Materials in Medicine*, *29*(9), 1-12.

38. Cardenas-Triviño, G., & Carrasco-Garcia, G. (2019). Chitosan composites prepared with hydroxyapatite and lactic acid as bone substitute. *Journal of the Chilean Chemical Society*, *64*(4), 4613-4618.

39. Danylchenko, S. M., Kalinkevich, O. V., & Pogorelov, M. V. (2009). Chitosan–hydroxyapatite composite biomaterials made by a one step co-precipitation method: preparation, characterization and in vivo tests.

40. Ahmed, G. M., Abouauf, E. A., AbuBakr, N., Dörfer, C. E., & El-Sayed, K. F. (2020). Tissue Engineering Approaches for Enamel, Dentin, and Pulp Regeneration: An Update. *Stem cells international*, *2020*, 5734539. https://doi.org/10.1155/2020/5734539

41. Bottino, M. C., Pankajakshan, D., & Nör, J. E. (2017). Advanced Scaffolds for Dental Pulp and Periodontal Regeneration. *Dental clinics of North America*, *61*(4), 689–711. https://doi.org/10.1016/j.cden.2017.06.009

42. Zhu, Y., Wan, Y., Zhang, J., Yin, D., & Cheng, W. (2014). Manufacture of layered collagen/chitosan-polycaprolactone scaffolds with biomimetic microarchitecture. *Colloids and Surfaces B: Biointerfaces*, *113*, 352-360.

43. Aranaz, I., Martínez-Campos, E., Moreno-Vicente, C., Civantos, A., García-Arguelles, S., & Del Monte, F. (2017). Macroporous Calcium Phosphate/Chitosan Composites Prepared via Unidirectional Ice Segregation and Subsequent Freeze-Drying. *Materials (Basel, Switzerland)*, *10*(5), 516. https://doi.org/10.3390/ma10050516

44. Chen, W., Zhou, H., Tang, M., Weir, M. D., Bao, C., & Xu, H. H. (2012). Gas-foaming calcium phosphate cement scaffold encapsulating human umbilical cord stem cells. *Tissue engineering. Part A*, *18*(7-8), 816–827. https://doi.org/10.1089/ten.TEA.2011.0267

45. Thein-Han, W., & Xu, H. H. (2013). Prevascularization of a gas-foaming macroporous calcium phosphate cement scaffold via coculture of human umbilical vein endothelial cells and osteoblasts. *Tissue engineering. Part A*, *19*(15-16), 1675–1685. https://doi.org/10.1089/ten.TEA.2012.0631

46. Chen, W., Thein-Han, W., Weir, M. D., Chen, Q., & Xu, H. H. (2014). Prevascularization of biofunctional calcium phosphate cement for dental and craniofacial repairs. *Dental materials : official publication of the Academy of Dental Materials*, *30*(5), 535–544. https://doi.org/10.1016/j.dental.2014.02.007

47. Dorozhkin S. V. (2012). Dissolution mechanism of calcium apatites in acids: A review of literature. *World journal of methodology*, *2*(1), 1–17. https://doi.org/10.5662/wjm.v2.i1.1

48. Shakir, M., Jolly, R., Khan, M. S., Iram, N. E., Sharma, T. K., & Al-Resayes, S. I. (2015). Synthesis and characterization of a nano-hydroxyapatite/chitosan/polyethylene glycol nanocomposite for bone tissue engineering. *Polymers for Advanced Technologies*, *26*(1), 41-48.

49. Kar, S., Kaur, T., & Thirugnanam, A. (2016). Microwave-assisted synthesis of porous chitosan–modified montmorillonite–hydroxyapatite composite scaffolds. *International journal of biological macromolecules*, *82*, 628-636.

50. Keikhaei, S., Mohammadalizadeh, Z., Karbasi, S., & Salimi A. (2019). Evaluation of the effects of β-tricalcium phosphate on physical, mechanical and biological properties of Poly (3-hydroxybutyrate)/chitosan electrospun scaffold for cartilage tissue engineering applications. *Materials Technology*, 34:10, 615-625. DOI: 10.1080/10667857.2019.1611053

51. Xin, R., Leng, Y., Chen, J., & Zhang, Q. (2005). A comparative study of calcium phosphate formation on bioceramics in vitro and in vivo. *Biomaterials*, *26*(33), 6477–6486. https://doi.org/10.1016/j.biomaterials.2005.04.028

52. Castro, N. J., Tan, W. N., Shen, C., & Zhang, L. G. (2016). Simulated Body Fluid Nucleation of Three-Dimensional Printed Elastomeric Scaffolds for Enhanced Osteogenesis. *Tissue engineering. Part A*, *22*(13-14), 940–948. https://doi.org/10.1089/ten.TEA.2016.0161

53. Shin, K., Acri, T., Geary, S., & Salem, A. K. (2017). Biomimetic Mineralization of Biomaterials Using Simulated Body Fluids for Bone Tissue Engineering and Regenerative Medicine. *Tissue engineering. Part A*, *23*(19-20), 1169–1180. https://doi.org/10.1089/ten.TEA.2016.0556

54. Yuan, X., Mak, A. F., & Li, J. (2001). Formation of bone-like apatite on poly(L-lactic acid) fibers by a biomimetic process. *Journal of biomedical materials research*, *57*(1), 140–150. https://doi.org/10.1002/1097-4636(200110)57:1<140::aid-jbm1153>3.0.co;2-g

55. An, S., Gao, Y., Ling, J., Wei, X., & Xiao, Y. (2012). Calcium ions promote osteogenic differentiation and mineralization of human dental pulp cells: implications for pulp capping materials. *Journal of materials science. Materials in medicine*, *23*(3), 789–795. https://doi.org/10.1007/s10856-011-4531-0

56. Gandolfi, M. G., Siboni, F., Botero, T., Bossù, M., Riccitiello, F., & Prati, C. (2015). Calcium silicate and calcium hydroxide materials for pulp capping: biointeractivity, porosity, solubility and bioactivity of current formulations. *Journal of applied biomaterials & functional materials*, *13*(1), 43–60. https://doi.org/10.5301/jabfm.5000201

57. Kuzmenka, D., Sewohl, C., König, A., Flath, T., Hahnel, S., Schulze, F. P., Hacker, M. C., & Schulz-Siegmund, M. (2020). Sustained Calcium(II)-Release to Impart Bioactivity in Hybrid Glass Scaffolds for Bone Tissue Engineering. *Pharmaceutics*, *12*(12), 1192. https://doi.org/10.3390/pharmaceutics12121192

58. Farhadian, N, Godiny, M., Moradi, S., Azandaryani, A. H., Shahlaei, M. (2018). Chitosan/gelatin as a new nano-carrier system for calcium hydroxide delivery in endodontic applications: Development, characterization and process optimization. *Materials Science and Engineering: C*, 92, 540-546. https://doi.org/10.1016/j.msec.2018.07.002.

59. Flores-Arriaga, J. C., Pozos-Guillén, A. J., González-Ortega, O., Escobar-García, D. M., Masuoka-Ito, D., Del Campo-Téllez, B., & Cerda-Cristerna, B. I. (2019). Calcium sustained release, pH changes and cell viability induced by chitosan-based pastes for apexification. *Odontology*, *107*(2), 223–230. https://doi.org/10.1007/s10266-018-0389-7

60. Boone, P. S., Zimmerman, M. C., Gutteling, E., Lee, C. K., Parsons, J. R., & Langrana, N. (1989). Bone attachment to hydroxyapatite coated polymers. Journal of biomedical materials research, 23(A2 Suppl), 183–199.

61. Al-Munajjed, A. A., Plunkett, N. A., Gleeson, J. P., Weber, T., Jungreuthmayer, C., Levingstone, T., Hammer, J., & O'Brien, F. J. (2009). Development of a biomimetic collagen-hydroxyapatite scaffold for bone tissue engineering using a SBF immersion technique. *Journal of biomedical materials research. Part B, Applied biomaterials*, *90*(2), 584–591. https://doi.org/10.1002/jbm.b.31320

Figures

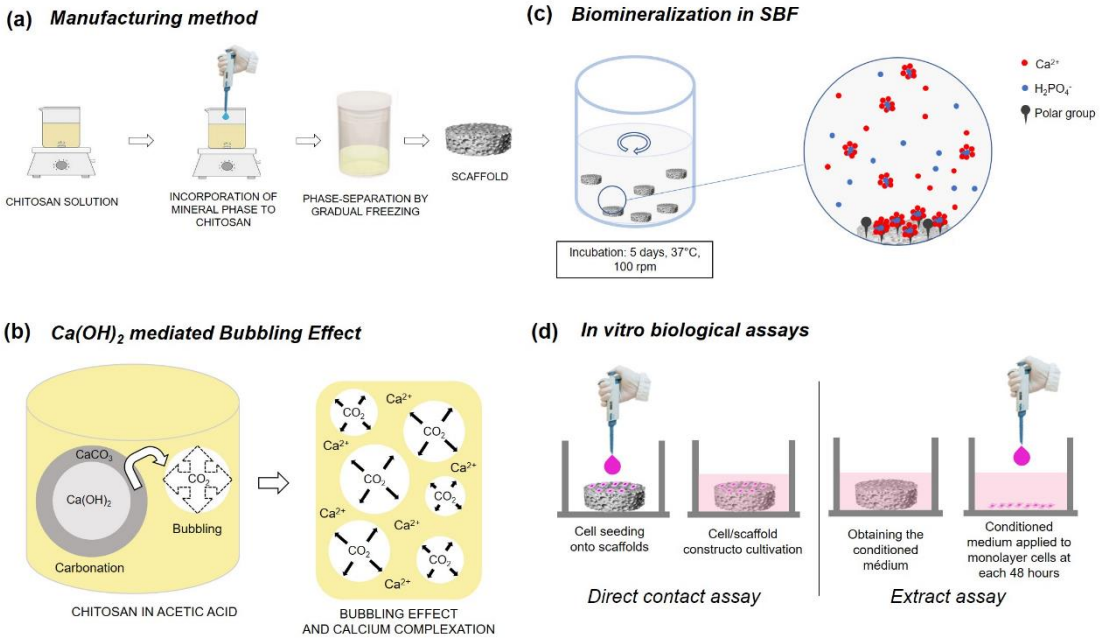

Figure 1. Representative schematics of manufacturing method (a), $Ca(OH)_2$ mediated Bubbling Effect (b), biomineralization in SBF (c) and in vitro biological methods (d).

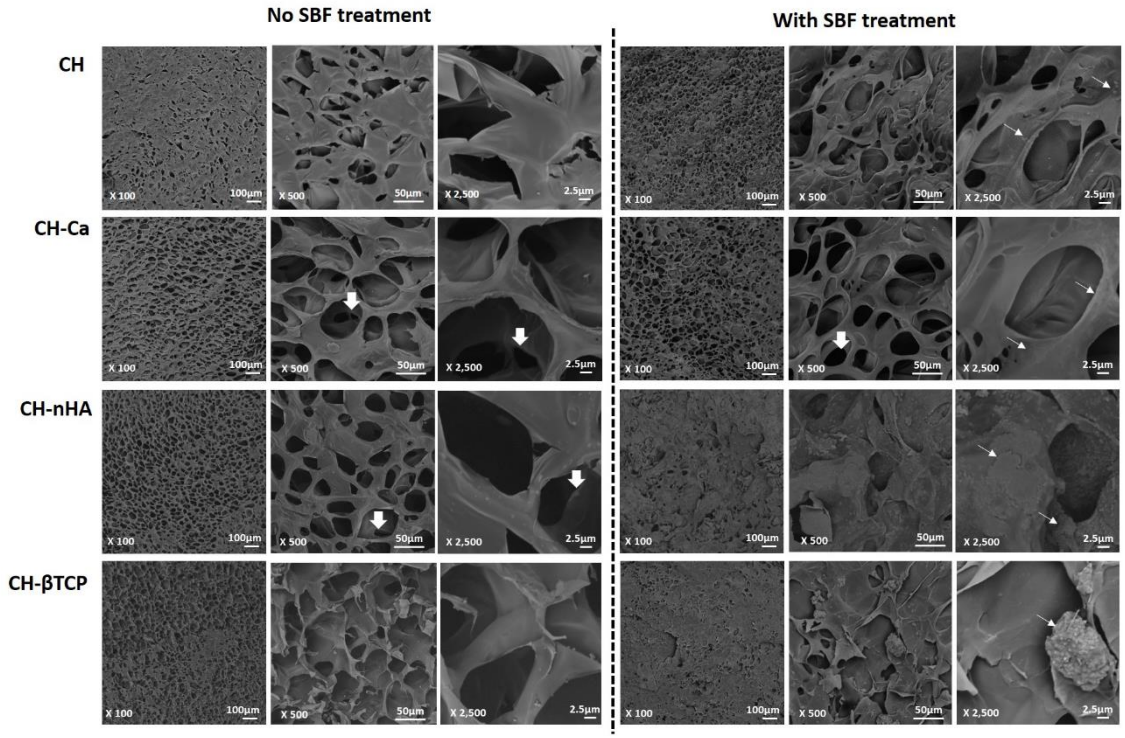

Figure 2. Scaffold architecture. SEM images of the surfaces of scaffolds subjected or not to SBF treatment. Magnifications of 100x, 500x, and 2500x. Note the round and well-organized pore network on CH-Ca and CH-nHA scaffolds not treated with SBF. Pore interconnectivity is indicated by large white arrows. CH-Ca treated with SBF maintained this porous network. Slight and sparse deposition of mineral-like structure is seen in SBF-treated CH and CH-Ca scaffolds (arrows). Mineral deposits can be easily detected on CH-nHA and CH-βTCP scaffolds treated with SBF (arrows), along with a disorganized and low porous architecture.

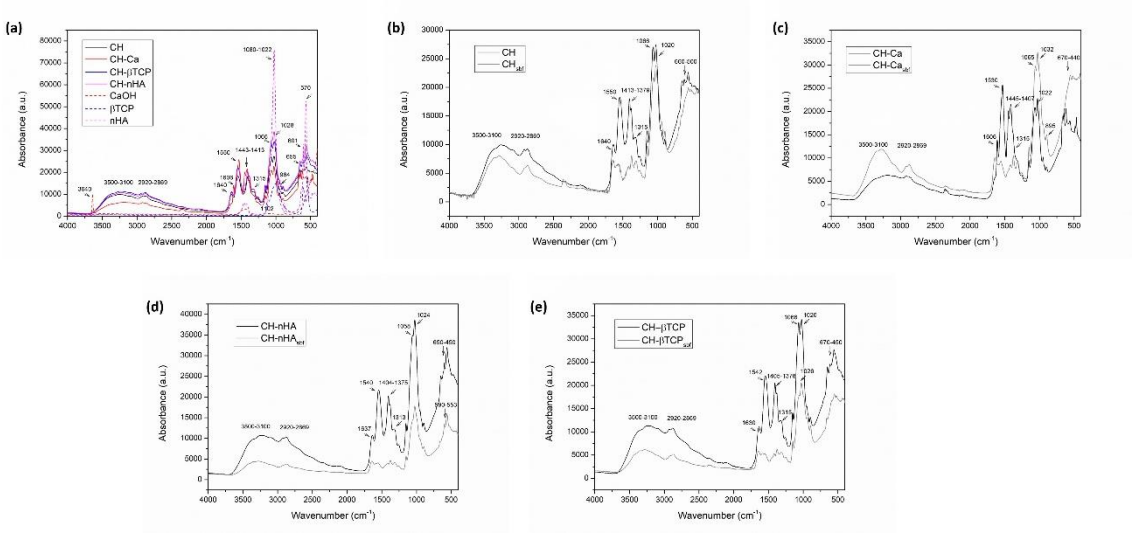

Figure 3. Chemical composition. Comparison of FTIR spectra after addition of mineral phases (a) and before and after incubation in SBF: CH and CH_{SBF} (b); CH-Ca and $CH\text{-}Ca_{SBF}$ (c); CH-nHA and $CH\text{-}nHA_{SBF}$ (d); CH-βTCP and $CH\text{-}\beta TCP_{SBF}$ (e).

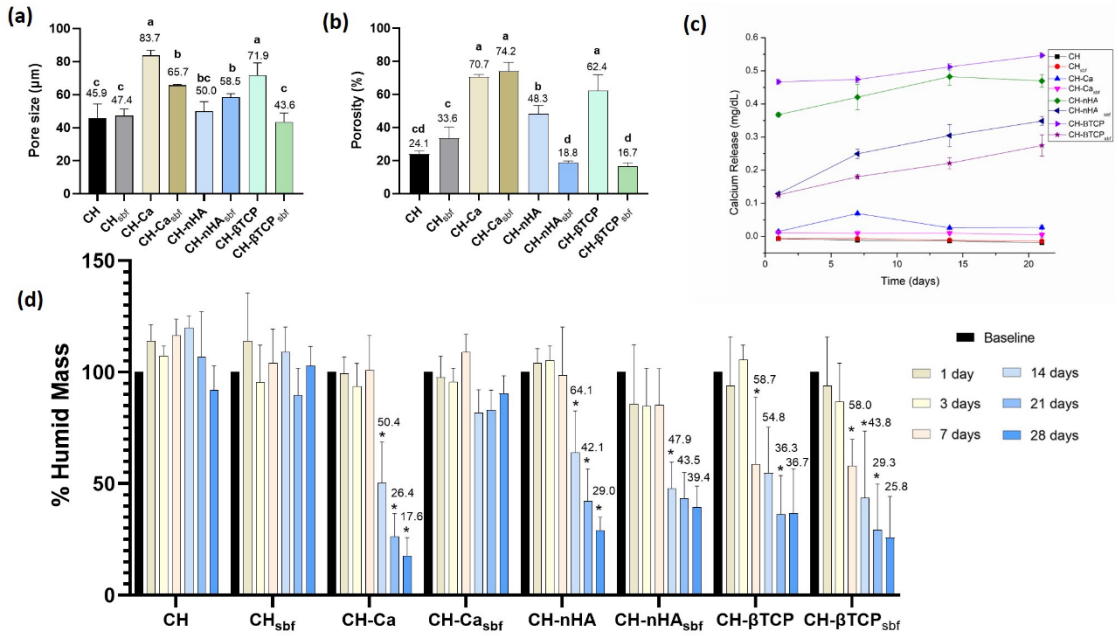

Figure 4. Physical characterization. Bar graph representing the mean values of pore size (a) and porosity degree (b). Numbers are mean values. Different letters indicate statistically significant differences among the groups (one-way ANOVA/Tukey´s test; $p < .05$). (c) Graph representative of mean and standard deviation values of cumulative calcium release (mg/dL) at 1, 7, 14, and 21 days. (d) Bar graph representing the mean humid mass % values. *Statistically significant difference from the immediately preceding analysis period (one-way ANOVA/Dunnett's test; $p < .05$)

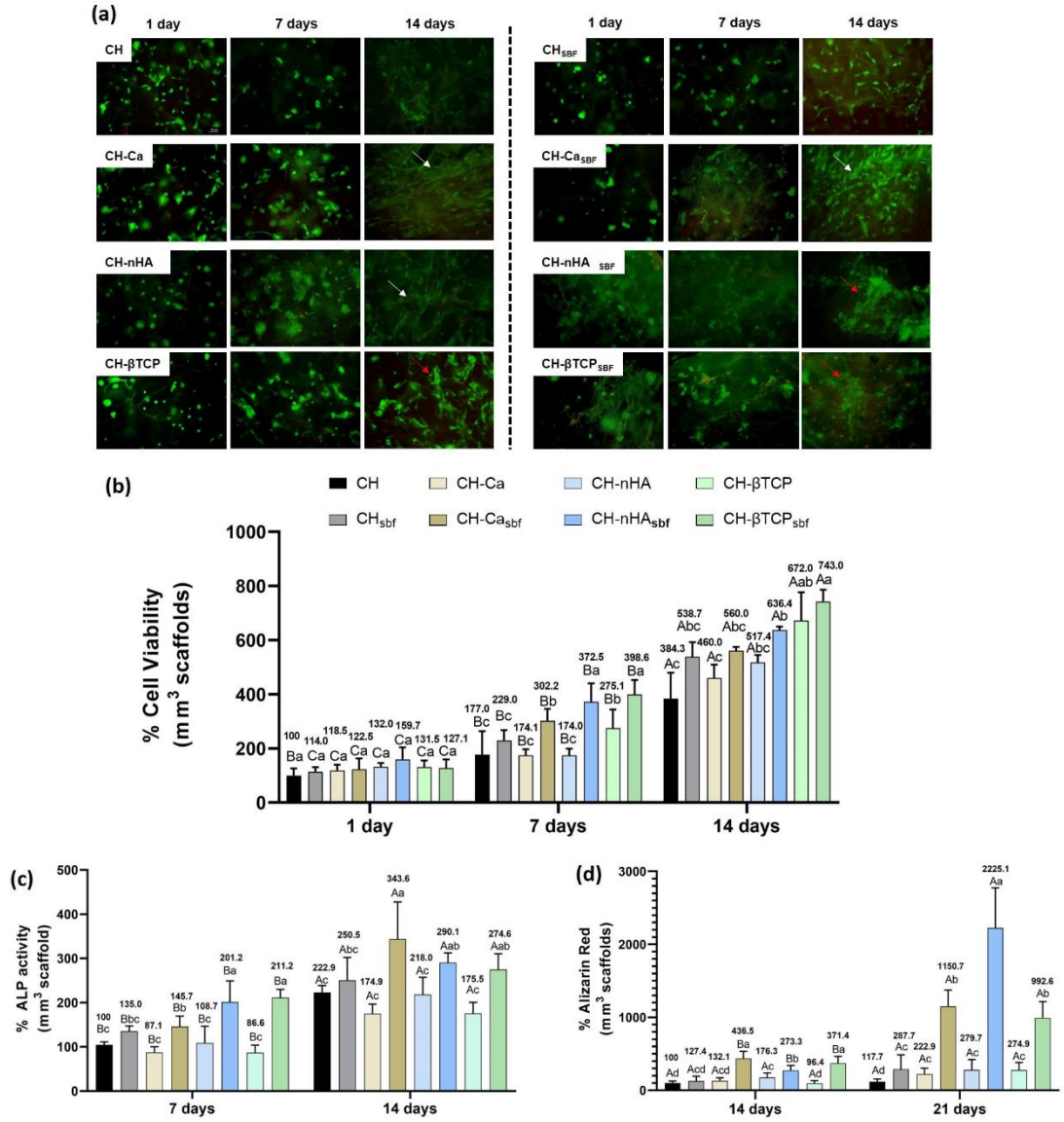

Figure 5. Direct contact assay. (a) Representative images of the Live/Dead assay. Green, viable cells; red, dead cells. 20x magnification. White arrows indicate cells with stretched cytoplasm. Red arrows indicate cells in agglomerates. (b, c, d) Alamar Blue assay, ALP activity, and Alizarin red assays, respectively. Bar graph representing the mean values (numbers). Capital letters allow for comparisons among the time-points for each experimental group. Lower-case letters allow for comparisons between and among experimental groups within each time-point. Different letters indicate statistically significant differences (RM two-way ANOVA/Tukey's test; $p < .05$)

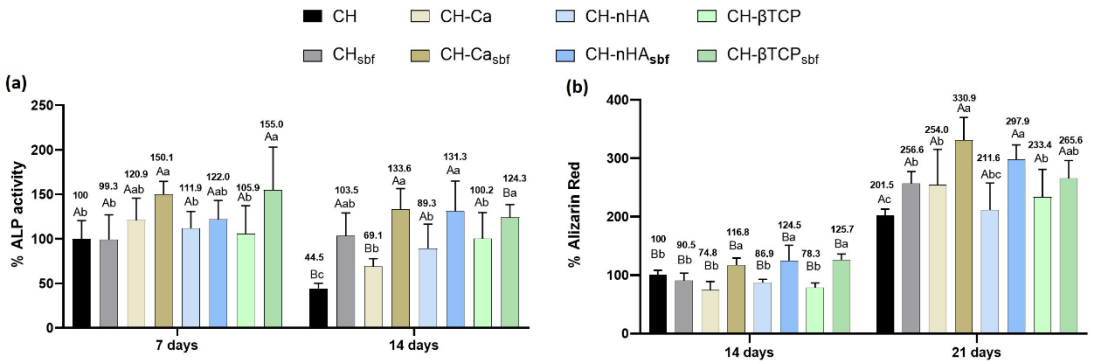

Figure 6. Conditioned medium assay. (a, b) ALP activity and Alizarin red assays, respectively. Bar graph representing the mean values (numbers). Capital letters allow for comparisons between the analysis periods for each experimental group. Lower-case letters allow for comparisons between and among experimental groups within each period of analysis. Different letters indicate statistically significant differences (two-way ANOVA/Tukey's test; $p < .05$)